RESEARCH ARTICLE | DECEMBER 17 2024

Clock transitions generated by defects in silica glass

Special Collection: Defects in Solids for Quantum Technologies

Brendan C. Sheehan ; Guanchu Chen ; Jonathan R. Friedman

Appl. Phys. Lett. 125, 254003 (2024)
https://doi.org/10.1063/5.0239469
CHORUS

Applied Physics Letters ARTICLE pubs.aip.org/aip/apl

Clock transitions generated by defects in silica glass

Cite as: Appl. Phys. Lett. **125**, 254003 (2024); doi: 10.1063/5.0239469
Submitted: 19 September 2024 · Accepted: 5 December 2024 ·
Published Online: 17 December 2024

Brendan C. Sheehan,[1,2,a)] Guanchu Chen,[1,2] and Jonathan R. Friedman[1,2]

AFFILIATIONS

[1]Department of Physics and Astronomy, Amherst College, Amherst, Massachusetts 01002, USA
[2]Department of Physics, University of Massachusetts Amherst, Amherst, Massachusetts 01003, USA

Note: This paper is part of the Special Topic, Defects in Solids for Quantum Technologies.
[a)]**Author to whom correspondence should be addressed:** bcsheehan@umass.edu

ABSTRACT

Clock transitions (CTs) in spin systems, which occur at avoided level crossings, enhance quantum coherence lifetimes T_2 because the transition becomes immune to the decohering effects of magnetic field fluctuations to first order. We present the first electron-spin resonance characterization of CTs in certain defect-rich silica glasses, noting coherence times up to 16 μs at the CTs. We find CT behavior at zero magnetic field in borosilicate and aluminosilicate glasses, but not in a variety of silica glasses lacking boron or aluminum. Annealing reduces or eliminates the zero-field signal. Since boron and aluminum have the same valence and are acceptors when substituted for silicon, we suggest the observed CT behavior could be generated by a spin-1 boron vacancy center within the borosilicate glass, and similarly, an aluminum vacancy center in the aluminosilicate glass.

Quantum information science relies on qubits—two-level systems with energy levels that can be superposed for an amount of time useful for quantum operations to be implemented. In recent years, an explosion of interest in quantum information science has yielded proof-of-concept experiments and more, indicating an attractive future for quantum technologies. Commonly studied qubit technologies include superconducting circuits based on Josephson junctions,[1] trapped ion qubits,[2] defect-in-material spin qubits,[3] nuclear spin qubits,[4] molecular nanomagnets,[5–7] and hybrid architectures containing more than one type of qubit.[8–11] Because many of these systems can be manipulated and read out using spin resonance-type techniques, electronic spin states represent viable qubit platforms for quantum information processing using electron-spin resonance (ESR).[12–15] Some of these ESR-addressable systems have been shown to have phase memory times long enough to be useful for quantum gate operations and for storage of quantum information.

Clock transitions (CTs) in spin systems can further enhance quantum coherence by protecting the qubit from the environmental spin bath[16–20] and can be used for both single-qubit and multi-qubit gates.[21] A CT occurs at an avoided level crossing where $\nabla_{\mathbf{B}}\omega = \mathbf{0}$; the level transition frequency ω is therefore immune to the decohering effects of small magnetic field fluctuations to first order. Here, we present a study of previously undiscovered zero-field CTs in certain types of defect-rich structural silica glasses. In these CTs, we find coherence times over 15 μs, a value that makes these systems attractive as potential qubits or as quantum memory platforms for holographic information storage.[22,23] Furthermore, the zero-field nature of these CTs permits convenient coupling to superconducting qubit systems and therefore integration into a hybrid quantum architecture.[24] While the underlying physics of these CTs is not yet definitively determined, we present evidence to support the hypothesis that the CTs arise from spin-1 boron vacancy or aluminum vacancy centers within the silica matrix. Engineering of these silica glasses by compositional and production control could further enhance coherence at their CTs.

Silica glass is the glass form of quartz, made of SiO_2 in an amorphous solid. The magnetic properties of defects in quartz and other forms of silica have been studied over the years for a number of different purposes, including thermal,[25] optical,[26] and magnetic[27,28] properties, and generation of spin-1/2 E′ centers via implantation and irradiation.[29–31] Spin systems in quartz after irradiation, however, tend to be spin-1/2 systems with a Zeeman-like Hamiltonian and $g \sim 2$. Furthermore, many borosilicate glasses and quartzes have iron (Fe^{3+}) impurities, which are interstitial defects with an electronic $S = 5/2$ and $g \approx 4.3$. Silica glasses have previously been shown to have vacancies,

as well, including charged oxygen vacancies.[32,33] Still other glasses, including several of the glasses examined for the current study, have been examined for zero-field increase in polarization echoes, which were not used to quantify spin coherence.[34,35] The potential of these systems for use as spin qubits has not yet been examined. One attractive feature of silica for quantum coherence is that of the stable isotopes of silicon and oxygen, only ^{29}Si (4.685% natural abundance) and ^{17}O (0.0373%) have nuclear spin, so the glass matrix intrinsically has very low nuclear magnetic noise.

Although the energy-level structure of the CT spin system in silica is not yet fully characterized, we provide a heuristic model of an avoided crossing at zero field. Generation of an avoided crossing at zero field requires a system with integer spin due to Kramers's theorem; here, we employ a model of a spin-1 system with Hamiltonian given by

$$\mathscr{H} = -DS_z^2 + E(S_x^2 - S_y^2) + g_s\mu_B \boldsymbol{B}\cdot\boldsymbol{S}. \tag{1}$$

The first and second terms represent longitudinal and transverse anisotropies, respectively, and the third term is the Zeeman interaction with the magnetic field. In the $\hat{S}_z$ basis, the energy eigenstates at zero field are

$$\begin{aligned} |+\rangle &= (|1\rangle + |-1\rangle)/\sqrt{2}, \\ |-\rangle &= (|1\rangle - |-1\rangle)/\sqrt{2}, \\ |0\rangle & \end{aligned} \tag{2}$$

with energies $-D+E$, $-D-E$, and 0, respectively. When $D \gg E$, the avoided crossing between the $|+\rangle$ and $|-\rangle$ states becomes an effective two-level system. The energy splitting of the avoided crossing is therefore $2E$, and ESR radiation applied such that $\hbar\omega = 2E$ addresses the CT.

Figure 1(a) shows the energy-level diagram calculated from the eigenstates of Eq. (1) with $D = 21$ GHz and $E = 2.25$ GHz and assuming $\vec{B} \parallel \hat{z}$. The states drawn in red and blue approach the $|+\rangle$ and $|-\rangle$ states as the field is tuned to zero; these states constitute the two levels addressed in ESR experiments. Our measurements do not provide sufficient information to determine the magnitude or sign of D (Fig. S8 and related discussion in the supplementary material). In our experiments, we observe a substantial range of ESR frequencies that give rise to CT behavior at zero field, from ∼3.5 to 5.5 GHz. Within this range, the signal amplitude and spin dynamics at the CT is largely unchanged. This indicates significant inhomogeneity in the transverse anisotropy such that at any given ESR frequency only a small subensemble of the total spins in the sample is addressed (Fig. S5). We therefore include a Gaussian distribution in E, centered on $E = 2.25$ GHz with a FWHM of 1.0 GHz, into our heuristic model. Figure 1(b) [corresponding to the dashed black box in (a)] shows the avoided crossing generated by this distribution. The intensity of the color for both states corresponds to the density of spins at each E value in the distribution. The black arrows indicate the range of frequencies over which the CT is observed to be strongest. The large inhomogeneous broadening we observe may arise from a single defect that is highly susceptible to the structural strains intrinsic to the amorphous matrix. Alternatively, numerous defect centers, each with its own CT frequency, may contribute to the ensemble, but would all need to have similar spin relaxation dynamics.

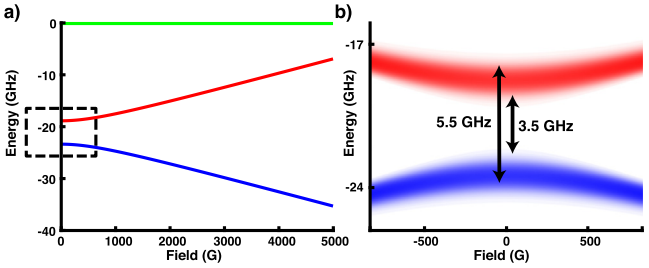

FIG. 1. Level diagrams of a spin-1 system. (a) An energy-level diagram of a spin-1 system. Green represents the $|0\rangle$ state, while red and blue, the two lowest-lying states, form an avoided crossing. The level diagram was calculated using Eq. (1) with $D = 21$ GHz and $E = 2.25$ GHz. (b) The inhomogeneously broadened avoided crossing near zero field, corresponding to the region within the dashed box in (a). This inhomogeneous broadening was calculated with a Gaussian distribution in E with a FWHM of 1.0 GHz. Inhomogeneous broadening in E provides a mechanism of generating a broadband CT, matching the behavior observed in this study. The arrows represent the edges of the frequency range over which we measure the CT.

To perform ESR experiments, all samples were mounted into a loop-gap resonator (LGR)[36,37] made of OFHC copper and held in place with a small quantity of vacuum grease (the vacuum grease gives no ESR signal and causes no observable change in the Q). Measurements were done using a home-built ESR probe with *in situ* frequency and coupling tunability[38] within a Quantum Design Physical Property Measurement System (PPMS) with a base temperature of 1.8 K. Typically, our resonators have a high quality factor ($Q \sim 2000$ at low temperature); for pulse ESR experiments, a small quantity of Eccosorb-brand microwave absorber was placed near the resonator to reduce the Q and shorten ringdown. For all experiments reported herein, the LGR was mounted into the probe such that the microwave $\vec{B}_1$ field of the resonator was parallel to the DC field $\vec{B}_0$. The spectrometer was built from commercially available microwave circuit components; microwave pulses were generated via the programmable Tabor SE5082 Arbitrary Waveform Generator (AWG) and echoes were measured via a homodyne technique and digitized using an oscilloscope. To remove background signals, we employed a four-step phase-cycling process.

Table I provides chemical compositions for glass samples examined in this study. Duran is a brand name for borosilicate glass 3.3 (DIN ISO 3585); aluminosilicate 0812 is manufactured by Schott;

TABLE I. Composition of each glass sample studied, as percentage by mass. All data were sourced from commercially available descriptions of the material from the supplier. The asterisk (*) for Duran indicates that Schott provides the measure of 4% by mass for the combination $Na_2O + K_2O$. We note that we could not source precise compositional information for one other borosilicate glass sample with an observed CT; this sample is termed "borosilicate" in this manuscript. Composition data for samples that did not exhibit zero-field ESR signal are given in Table S1.

	Duran	Aluminosilicate 0812	Vycor 7913	AGC40
SiO_2 (%)	81	60	96	95
B_2O_3 (%)	13	4.5	3	5
Al_2O_3 (%)	2	14	0	Trace
Na_2O (%)	4*	<0.02	Trace	Trace
K_2O (%)	4*	0	0	0
CaO (%)	0	10	0	0
BaO (%)	0	9	0	0

Vycor 7913 was manufactured by Corning; and AGC40 is manufactured by Advanced Glass and Ceramics to mimic the physical properties of Vycor 7913. Both Vycor 7913 and AGC40 are porous borosilicate glass. One sample, that we simply call "borosilicate" glass, was sourced from McMaster-Carr, which is a distributor, not a manufacturer. The provenance and detailed chemical characterization of that sample are not established.

Figure 2(a) shows the results of studying Duran glass (13% B_2O_3-in-SiO_2), red, a "borosilicate" glass sample, black, and a sample of 0812 aluminosilicate glass, blue, using pulsed ESR in an echo-detected field sweep (EDFS) experiment. A standard Hahn echo sequence was used. All three samples show a clearly defined zero-field peak, although the aluminosilicate's peak is wider with a cusp at zero field while the Duran's and borosilicate's peaks are more rounded. While the data for each sample shown in Fig. 2(a) were taken at a different microwave frequency, we have not noted any appreciable difference in sample behavior within a wide range of frequencies—see discussion of Fig. 1(b). Figure S4 shows examples of the CT being addressed across the range ∼3.5–∼ 5.1 GHz; each CT demonstrates qualitatively similar behavior throughout. A Vycor 7913 sample also showed a zero-field-peaked ESR signal, albeit much weaker than that found in other glass samples that showed CTs (Fig. S3).

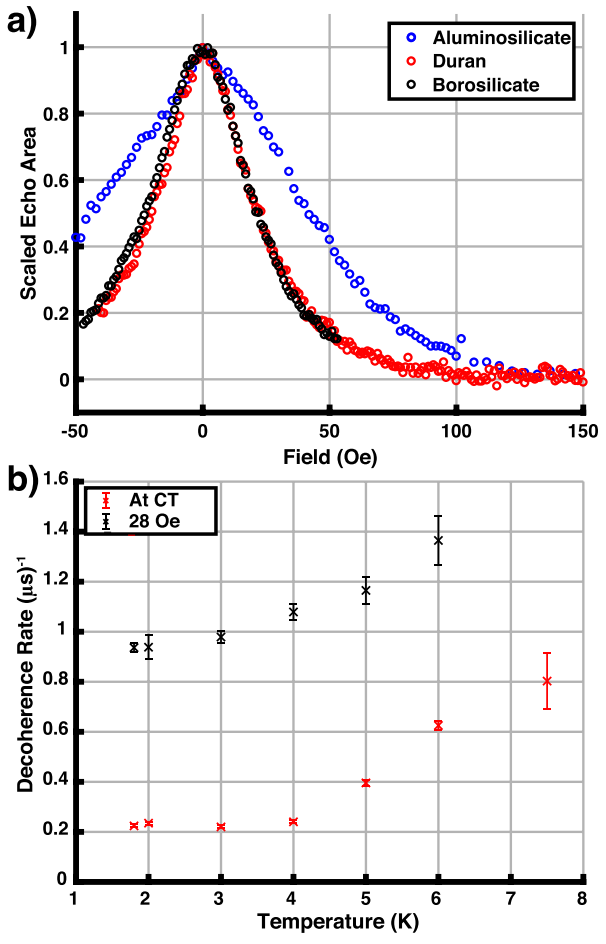

FIG. 2. Evidence of a Clock Transition in Glass Samples. (a) Echo response with a standard Hahn echo sequence near zero field of aluminosilicate glass (measured at 5036 MHz, delay time $\tau = 1000$ ns, blue), Duran glass (3975 MHz, $\tau = 800$ ns, red), and borosilicate glass (5117 MHz, $\tau = 1000$ ns, black). Measurements were taken at 1.8 K and at frequencies within the range of the inhomogeneously broadened CT (Fig. 1). (b) Decoherence rate measured with the Hahn echo sequence by varying τ at different temperatures at 0 Oe (red) and 28 Oe (black) in Duran glass at 3969 MHz.

To further characterize these signals, we study the coherence of these transitions by examining the dependence of the echo area on the delay time τ between the $\pi/2$ and π pulses. An example of this dependence is shown in Fig. S1(a). Figure 2(b) shows the decoherence rate $(1/T_2)$ measured in Duran glass at multiple temperatures and two fields (0 Oe in red and 28 Oe in black). The stark reduction of decoherence rate as the field is tuned to the zero-field peak confirms the CT effect. At the CT, notably, the decoherence rate exhibits a plateau below approximately 4 K. We note that phonon-driven dephasing should be temperature dependent; the underlying mechanism for the observed temperature-independent dephasing is unknown and is the subject of active investigation. We can rule out that the plateau is caused by radiative heating from the pulses since the echo amplitude does not have a similar plateau below 4 K [Fig. S8(b)].

Figure 3(a) shows T_2 for aluminosilicate (blue), Duran (red), and borosilicate (black) glasses. In each sample, T_2 is longest (up to ∼4 μs) at zero field, and falls off rapidly as the field is tuned away from zero. This observation is the hallmark of the CT effect: To first order, spins in the system are protected from the decohering effects of dipolar interactions and can therefore retain their phase coherence for longer. We have also observed Rabi oscillations at the CT in our samples (Fig. S2). By applying the Carr–Purcell–Meiboom–Gill (CPMG) pulse sequence, wherein repeated application of π pulses refocuses the spins via the sequence $(\pi/2)_x - (\tau - \pi_y - \tau - \text{echo})^N$ (for N integer; in this study $N = 20$), coherence can be further enhanced. The decay of the echo area as a function of total evolution time provides a measure of this enhanced T_2. Figure 3(b) shows that each sample exhibits enhanced coherence with the CPMG pulse sequence [when compared with the Hahn results of (a)]. An example of a CPMG trace is shown in Fig. S1(b). While all three samples show a clear CPMG enhancement of T_2, the effect is material dependent. Both borosilicate samples show similar T_2 from the Hahn experiment (a), but the Duran shows a much smaller CPMG enhancement in (b). The aluminosilicate shows the largest enhancement, with coherence times measured by CPMG exceeding 15 μs. We note that the aluminosilicate sample also shows a series of small side peaks, seen most clearly in Fig. 3(b) between 10 and 20 Oe—perhaps arising from hyperfine coupling to the ^{27}Al nuclear spin—but these were not investigated in detail in this study (however, we do observe ESEEM from ^{11}B in a borosilicate sample—see Fig. S7).

Figure 3(c) shows the ratio $(T_{2,\text{CPMG}}/T_{2,\text{Hahn}})$ of coherence times measured in Figs. 3(a) and 3(b) for all three glass samples as a function of magnetic field. Each sample behaves differently: though both borosilicate (black) and Duran (red) show that CPMG is less effective at enhancing coherence at the CT than when the field is tuned away, Duran shows that CPMG only improves coherence by a factor of 1.5 at the CT. One interpretation is that as this ratio approaches unity at the CT, CPMG becomes partially redundant as a decoherence noise filter since the CT already filters low-frequency magnetic noise

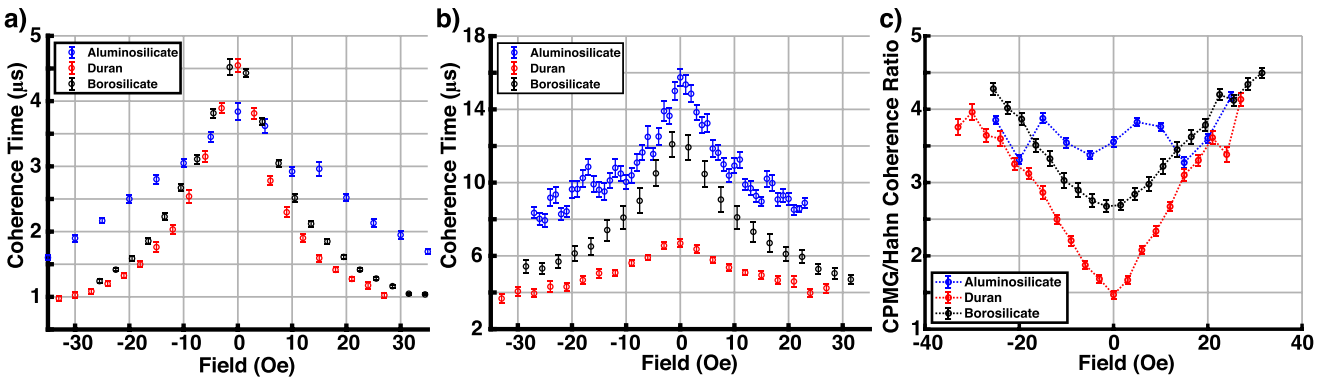

FIG. 3. Coherence near zero field. (a) Increase in coherence time, as measured via a Hahn echo sequence, near zero field. Aluminosilicate (blue), Duran (red), and borosilicate (black) glasses all show a peak at zero field. When paired with the data in Fig. 2(a), these data have the hallmarks of a zero-field CT: enhanced echo signal and coherence. (b) T_2 measured via the CPMG pulse sequence, with 20 π-pulses, for the same three samples (with delay $\tau = 1000$ ns for aluminosilicate and borosilicate, and $\tau = 800$ ns for Duran). (c) The ratio of T_2 measured by CPMG to T_2 measured by Hahn echo, for all three glass samples. Measurements occurred at 1.8 K, with ESR frequencies of 5036 MHz (aluminosilicate), 4028 MHz (Duran), and 5117 MHz (borosilicate).

(Figure S9 shows the noise spectrum at and 30 Oe away from the CT determined from CPMG data on a Duran glass sample). This suggests that the primary source of decoherence in this material is low-frequency magnetic noise. Aluminosilicate (blue) shows no such relationship—no clear trend in the ratio of coherence times can be seen as the field is tuned through the CT.

One commonality among many of the samples exhibiting the CT effect is the presence of both SiO_2 and boron as a substitutional defect. Thus, we examined multiple borosilicate glasses with differing boron concentrations. Figure 4 shows a comparison of 5% B_2O_3 in SiO_2 (in blue, AGC40) and Duran glass [also shown in Fig. 2(a) in red], overlaid. At zero field, the echo area is substantially reduced in the dilute sample, suggesting that the spin system producing the CT has been

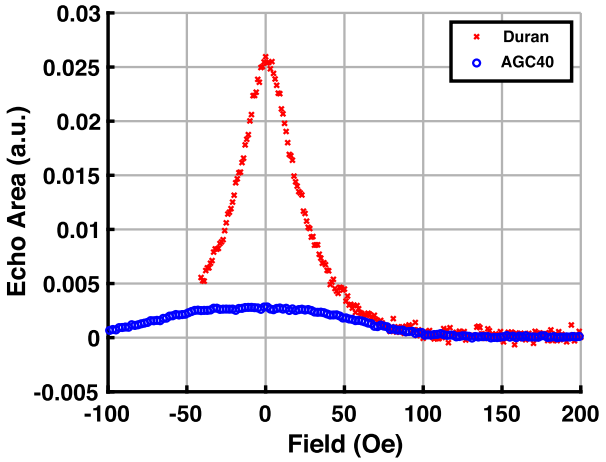

FIG. 4. Comparison of EDFS at the CT with different concentrations of boron. Echo area, from a standard Hahn sequence with delay $\tau = 1000$ ns, as a function of magnetic field near the CT for two samples of borosilicate glass, showing different intensity of the peak at the CT. In red, the CT for Duran glass is shown (measured at 1.8 K and 3975 MHz); in blue, the CT for the AGC40 glass (1.8 K and 3773 MHz) shows much smaller echo signal at zero field.

reduced. The ratio of signal sizes is not 13:5, as one might initially expect. Part of this may be due to small changes in experimental conditions that change absolute signal size between experimental runs. Nevertheless, there are clearly other differences between the two samples with the peak for AGC40 being wider and having a much flatter top than for Duran. One confounding factor is the porosity of AGC40, which makes direct comparison challenging. We observe shorter coherence at the CT in AGC40 (Fig. S6), which may be related to the porosity of the glass.

We also examined the behavior of each sample after annealing. Details of the annealing process for each annealed sample are provided in Table S2. AGC40, Vycor 7913, and aluminosilicate glass showed no detectable echo after annealing. Figure 5(a) shows a markedly reduced echo signal after annealing for the borosilicate; the echo signal at zero field is reduced by nearly 80%. This suggests that annealing the glass reduces the number of the spin centers generating the CT. Figure 5(b) shows a remarkable T_2 value of $\sim$16 μs at the CT as measured with CPMG, a 32% increase over the non-annealed sample. While annealing substantially reduced the CT signal for nearly all of our samples, one notable exception was the Duran sample, which showed no significant change. This distinction will be the subject of further investigation.

Our results demonstrate substantial coherence times in several glass samples, with T_2 enhanced at the zero-field CT. ESR response for our CT signal also appears to depend on boron concentration (e.g., Fig. 4). In addition, annealing reduces the response while simultaneously enhancing coherence. While annealing may have many effects on the properties of the glass, one well-known consequence of the annealing process is the removal of vacancies. Silica glasses and quartz are known to contain numerous vacancies, notably oxygen vacancies.[32,39] Our observations then suggest that vacancies potentially play a role in the spin system that is responsible for the CT. One hypothesis, then, for the microscopic source of the CT in the borosilicate glasses is a spin-1 boron vacancy (BV) center, and, for aluminosilicate glass, a spin-1 aluminum vacancy (AlV) center. Boron and aluminum, both in Group 13 of the periodic table, are electron acceptors when substituting for silicon. They therefore introduce a localized hole with spin-1/2 when doped into the glass. We hypothesize that when coupled to a

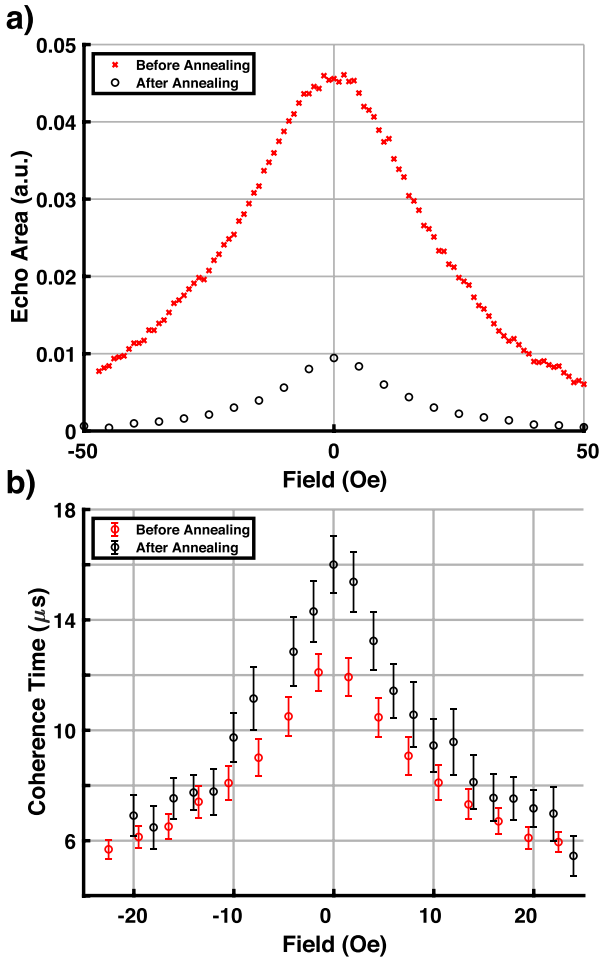

FIG. 5. Comparison of CT before and after annealing borosilicate glass. (a) A comparison of the echo area at the CT before (red, measured at 1.8 K and 5117 MHz) and after (black, measured at 1.8 K and 3836 MHz) annealing the sample. After annealing the sample, echo signal drops substantially at and away from the CT, suggesting that fewer spins in the annealed sample are being addressed by the ESR frequency. (b) Overlay of coherence times of the same samples as (a), measured by the CPMG pulse sequence, showing a ∼32% increase in T_2 at zero field after annealing the 13% borosilicate glass. All data in both panels used a delay time of $\tau = 1000$ ns. We kept the ESR frequency for all data shown restricted to within the frequency range of the inhomogeneously broadened CT.

neighboring charged oxygen vacancy that also has a spin-1/2, such defects can form a spin-1 system capable of producing a zero-field CT.

CTs in glass defects offer ample avenues for future exploration. In other quantum systems, chemical engineering has enabled alteration of the zero-field splitting[40] and enhanced spin coherence.[41] Through further materials study and engineering, these glasses may be exploited to further improve coherence. Furthermore, color centers have previously been observed in silica glasses in a number of contexts.[42–44] One tantalizing, but perhaps remote, possibility is that the spin system underpinning the CT may behave as an ESR-addressable color center in silica glass, a feature with obvious applications in quantum sensing, analogous to the well-known NV^- center in diamond, or more specifically the negatively charged BV center in diamond.[45,46]

See the supplementary material for Rabi oscillation measurements, examples of coherence time measurements, an example of a spectral hole-burning experiment, broadband CT characterization, a study of temperature dependence of the CT, discussion of the CPMG noise spectrum of Duran glass at and away from the CT, and details about the annealing processes.

The authors would like to thank G. Joshi and K.-I. Ellers for carrying out some preliminary experiments, J. Kubasek for assistance with machining the resonators used in this study, and B. Crepeau for assistance with instrumentation. C. A. Collett, I. Nikolov, F. Abdo Arias, T. Pathak, K. Thompson, and J. Levy provided useful conversations and advice. We are grateful to S. Prasch for help with annealing samples. This work was supported by the Research Corporation for Science Advancement under Cottrell SEED Award No. 27849 and by the National Science Foundation under Grant Nos. DMR-1708692 and DMR-2207624. JRF acknowledges the support of the Amherst College Senior Sabbatical Fellowship Program, which is funded in part by the H. Axel Schupf '57 Fund for Intellectual Life.

AUTHOR DECLARATIONS

Conflict of Interest

The authors have no conflicts to disclose.

Author Contributions

Brendan C. Sheehan: Conceptualization (equal); Formal analysis (lead); Investigation (equal); Methodology (equal); Software (equal); Visualization (equal); Writing – original draft (lead); Writing – review & editing (equal). **Guanchu Chen:** Conceptualization (equal); Investigation (supporting); Methodology (equal); Software (equal); Visualization (equal); Writing – review & editing (supporting). **Jonathan R. Friedman:** Conceptualization (lead); Funding acquisition (lead); Methodology (equal); Project administration (lead); Resources (lead); Supervision (lead); Writing – original draft (supporting); Writing – review & editing (equal).

DATA AVAILABILITY

The data that support the findings of this study are available from the corresponding author upon reasonable request.

REFERENCES

[1]M. Kjaergaard, M. E. Schwartz, J. Braumüller, P. Krantz, J. I.-J. Wang, S. Gustavsson, and W. D. Oliver, Annu. Rev. Condens. Matter Phys. **11**, 369 (2020).
[2]C. D. Bruzewicz, J. Chiaverini, R. McConnell, and J. M. Sage, Appl. Phys. Rev. **6**, 021314 (2019).
[3]J. J. L. Morton, D. R. McCamey, M. A. Eriksson, and S. A. Lyon, Nature **479**, 345 (2011).
[4]A. J. Heinrich, W. D. Oliver, L. M. K. Vandersypen, A. Ardavan, R. Sessoli, D. Loss, A. B. Jayich, J. Fernandez-Rossier, A. Laucht, and A. Morello, Nat. Nanotechnol. **16**, 1318 (2021).
[5]S. Takahashi, I. S. Tupitsyn, J. Van Tol, C. C. Beedle, D. N. Hendrickson, and P. C. E. Stamp, Nature **476**, 76 (2011).
[6]E. Coronado, Nat. Rev. Mater. **5**, 87 (2019).
[7]A. Chiesa, P. Santini, E. Garlatti, F. Luis, and S. Carretta, Rep. Prog. Phys. **87**, 034501 (2024).

[8]P. Rabl, D. DeMille, J. M. Doyle, M. D. Lukin, R. J. Schoelkopf, and P. Zoller, Phys. Rev. Lett. **97**, 033003 (2006).
[9]J. J. Morton and B. W. Lovett, Annu. Rev. Condens. Matter Phys. **2**, 189 (2011).
[10]A. A. Clerk, K. W. Lehnert, P. Bertet, J. R. Petta, and Y. Nakamura, Nat. Phys. **16**, 257 (2020).
[11]I. Gimeno, W. Kersten, M. C. Pallarés, P. Hermosilla, M. J. Martínez-Pérez, M. D. Jenkins, A. Angerer, C. Sánchez-Azqueta, D. Zueco, J. Majer, A. Lostao, and F. Luis, ACS Nano **14**(7), 8707–8715 (2020).
[12]F. Luis, F. L. Mettes, J. Tejada, D. Gatteschi, and L. J. De Jongh, Phys. Rev. Lett. **85**, 4377 (2000).
[13]M. N. Leuenberger and D. Loss, Nature **410**, 789 (2001).
[14]J. Tejada, E. M. Chudnovsky, E. del Barco, J. M. Hernandez, and T. P. Spiller, Nanotechnology **12**, 181 (2001).
[15]J. R. Friedman and M. P. Sarachik, Annu. Rev. Condens. Matter Phys. **1**, 109 (2010).
[16]G. Wolfowicz, A. M. Tyryshkin, R. E. George, H. Riemann, N. V. Abrosimov, P. Becker, H.-J. Pohl, M. L. W. Thewalt, S. A. Lyon, and J. J. L. Morton, Nat. Nanotechnol. **8**, 561 (2013).
[17]J. M. Zadrozny, J. Niklas, O. G. Poluektov, and D. E. Freedman, ACS Cent. Sci. **1**, 488 (2015).
[18]M. Shiddiq, D. Komijani, Y. Duan, A. Gaita-Ariño, E. Coronado, and S. Hill, Nature **531**, 348 (2016).
[19]C. Collett, K.-I. Ellers, N. Russo, K. Kittilstved, G. Timco, R. Winpenny, and J. Friedman, Magnetochemistry **5**, 4 (2019).
[20]K. Kundu, J. R. K. White, S. A. Moehring, J. M. Yu, J. W. Ziller, F. Furche, W. J. Evans, and S. Hill, Nat. Chem. **14**, 392 (2022).
[21]C. A. Collett, P. Santini, S. Carretta, and J. R. Friedman, Phys. Rev. Res. **2**, 032037 (2020).
[22]J. J. Morton and P. Bertet, J. Magn. Reson. **287**, 128 (2018).
[23]V. Ranjan, J. O'Sullivan, E. Albertinale, B. Albanese, T. Chanelière, T. Schenkel, D. Vion, D. Esteve, E. Flurin, J. J. L. Morton, and P. Bertet, Phys. Rev. Lett. **125**, 210505 (2020).
[24]Y. Kubo, C. Grezes, A. Dewes, T. Umeda, J. Isoya, H. Sumiya, N. Morishita, H. Abe, S. Onoda, T. Ohshima, V. Jacques, A. Dréau, J.-F. Roch, I. Diniz, A. Auffeves, D. Vion, D. Esteve, and P. Bertet, Phys. Rev. Lett. **107**, 220501 (2011).
[25]R. B. Stephens, Phys. Rev. B **13**, 852 (1976).
[26]D. L. Griscom, J. Ceram. Soc. Jpn. **99**, 923 (1991).
[27]G. Jug, M. Paliienko, and S. Bonfanti, J. Non-Cryst. Solids **401**, 66 (2014).
[28]G. Jug and S. Recchia, "Revealing the intrinsic magnetism of non-magnetic glasses," arXiv:2111.00614 (2021).
[29]R. A. Weeks, J. Non-Cryst. Solids **179**, 1–9 (1994).
[30]R. H. Magruder, A. Stesmans, R. A. Weeks, and R. A. Weller, J. Appl. Phys. **104**, 054110 (2008).
[31]T. Wang, X. Zhang, M. Sun, X. Du, M. Guan, H. Peng, and T. Wang, Nucl. Instrum. Meth. B **464**, 106 (2020).
[32]A. V. Kimmel and A. L. Shluger, J. Non-Cryst. Solids **355**, 1103 (2009).
[33]A. Kimmel, P. Sushko, A. Shluger, and G. Bersuker, ECS Trans. **19**, 3 (2009).
[34]S. Ludwig, P. Nagel, S. Hunklinger, and C. Enss, J. Low Temp. Phys. **131**, 89 (2003).
[35]P. Nagel, A. Fleischmann, S. Hunklinger, and C. Enss, Phys. Rev. Lett. **92**, 245511 (2004).
[36]W. Froncisz and J. S. Hyde, J. Magn. Reson. **47**, 515 (1982).
[37]E. R. Eisenach, J. F. Barry, L. M. Pham, R. G. Rojas, D. R. Englund, and D. A. Braje, Rev. Sci. Instrum. **89**, 094705 (2018).
[38]G. Joshi, J. Kubasek, I. Nikolov, B. C. Sheehan, T. A. Costa, R. A. Allão Cassaro, and J. R. Friedman, Rev. Sci. Instrum. **91**, 023104 (2020).
[39]L. Skuja, M. Hirano, H. Hosono, and K. Kajihara, Phys. Status Solidi C **2**, 15 (2005).
[40]D. W. Laorenza, A. Kairalapova, S. L. Bayliss, T. Goldzak, S. M. Greene, L. R. Weiss, P. Deb, P. J. Mintun, K. A. Collins, D. D. Awschalom, T. C. Berkelbach, and D. E. Freedman, J. Am. Chem. Soc. **143**, 21350 (2021).
[41]S. L. Bayliss, P. Deb, D. W. Laorenza, M. Onizhuk, G. Galli, D. E. Freedman, and D. D. Awschalom, Phys. Rev. X **12**, 031028 (2022).
[42]A. Amossov and A. Rybaltovsky, J. Non-Cryst. Solids **179**, 75 (1994).
[43]A. Amossov and A. Rybaltovsky, J. Non-Cryst. Solids **179**, 226 (1994).
[44]J. Du, J. Wu, L. Zhao, and L. Song, Radiat. Phys. Chem. **86**, 59 (2013).
[45]M. Muruganathan and H. Mizuta, Diam. Relat. Mater **114**, 108341 (2021).
[46]T. Umeda, K. Watanabe, H. Hara, H. Sumiya, S. Onoda, A. Uedono, I. Chuprina, P. Siyushev, F. Jelezko, J. Wrachtrup, and J. Isoya, Phys. Rev. B **105**, 165201 (2022).